Results in Engineering 32 (2026) 113675

Contents lists available at ScienceDirect

Results in Engineering

journal homepage: www.sciencedirect.com/journal/results-in-engineering

Research paper

Rapid evaluation of structural concepts in preliminary design of trailing-edge high-lift devices

Rakshith Manikandan *, David Zerbst, Erik Kappel, Lennart Tönjes, Edgar Werthen, Sascha Dähne, Christian Hühne

German Aerospace Center (DLR), Institute of Lightweight Systems, Lilienthalplatz 7, Braunschweig, 38108, Germany

ARTICLE INFO

Keywords:
CPACS
Beam-elements
High lift systems
Flap design
Structural sizing
Composite structures

ABSTRACT

This article introduces a rapid, mechanically informed design workflow for preliminary structural trade studies of control surfaces with composite materials. Developed to address the challenges of designing slender trailing-edge devices for high-aspect-ratio wings, the workflow enables systematic early-phase evaluation of alternative structural concepts. Flaperon geometries, parameterised with CPACS, are idealised using an efficient beam element solver, allowing simultaneous consideration of nominal aerodynamic loads and off-nominal kinematic failure loads. Structural responses under these loads are used to size the structure, ensuring compliance with strain, buckling, and deflection constraints. The workflow's utility is demonstrated through trade studies on representative inboard and outboard flaperons of the DLR-F25 research configuration. Mass sensitivities associated with support-station placement, number of spars, and their geometric layout are quantified to identify favourable design regions. Distinct optimal configurations emerge for bulky inboard and slender outboard flaperons, highlighting the geometry-dependent nature of structural decisions. As such, the presented workflow enables the rapid evaluation of structural concepts, supports cross-disciplinary exchanges, and facilitates context-specific decision-making in preliminary high-lift system design.

1. Introduction

The conceptual design of modern aircraft requires consistent integration of multiple disciplines under varying fidelity. Although early design phases offer significant architectural freedom, they are often guided by simplified constraints or rule-based margins, to ensure feasibility across subsequent phases [1]. Such constraints, usually driven by manufacturing considerations—e.g., minimum rear spar heights or geometric limits—are robust, but may obscure underlying physical sensitivities and limit exploration of superior alternate concepts. This effect is further compounded in a linear development processes, where key architectural decisions are fixed early. Parametric trade studies are therefore essential to challenge such constraints and enable informed, context-specific design decisions.

These challenges becomes particularly evident in the development of next-generation single-aisle aircraft, which target higher fuel efficiency, lower emissions, and reduced operating costs. High-aspect-ratio (HAR) wings (as illustrated in Fig. 1) are a key aerodynamic enabler in this context, offering reduced induced drag and improved cruise performance. However, their slender outboard geometry with control-surface profile heights as low as 5–10 cm [2], introduces significant structural and manufacturing challenges for trailing-edge (TE) high-lift devices. Conventional composite differential (or "skeleton") designs, consisting of ribs, spars, stiffened-skins, and closing elements assembled through riveting, remain the industrial baseline. Fig. 2a shows the individual parts of an A321 composite flap. Though the higher part counts offer flexibility with tolerance compensation, these architectures involve significant assembly effort. At projected production rates of up to 100 aircraft per month for future single-aisle platforms [3], such assembly efforts risks becoming a bottleneck. The reduced profile heights in HAR outboard regions further exacerbate accessibility and integration challenges.

In response, alternative modular and more integral reinforcement concepts have been proposed (Fig. 2b). High-Technical Readiness Level (TRL) approaches such as Composite Multi-Spar Flaps (CMF) and Advanced Multi-Cell Flaps (AMF) use dry-fiber preforms and resin transfer molding processes, yet require external load-introduction features (with box-opening or external fins) that increase geometric complexity. More recently, DLR's omega concept that is developed for a slender outboard flaperon of the F25 research configuration [2], aims to simplify manufacturing while maintaining structural efficiency. Here, all primary sub-laminates (skin, omega stiffener, and bottom cover) can be

* Corresponding author.
E-mail address: rakshith.manikandan@dlr.de (R. Manikandan).

https://doi.org/10.1016/j.rineng.2026.113675
Received 28 May 2026; Received in revised form 17 September 2026; Accepted 19 October 2026
Available online 23 October 2026
2590-1230/© 2026 The Author(s). Published by Elsevier B.V. This is an open access article under the CC BY-NC-ND license (http://creativecommons.org/licenses/by-nc-nd/4.0/).
Open access funding enabled and organized by Projekt DEAL.

manufactured from flat full-laminate stacks. Bracket accessibility is improved through a separately designed bottom panel.

Despite these developments, the structural implications and mass sensitivities of such concepts remain insufficiently quantified in early design phases. Fundamental architectural questions persist: Where should flaps be attached spanwise? How should spars be positioned chordwise? How many support stations are required, and how do these decisions vary with control-surface geometry? Can conventional rule-of-thumb solutions be extrapolated to HAR configurations? Handbook-based methods lack the fidelity to capture geometry-dependent sensitivities, while high-fidelity simulations are computationally intensive for broad concept exploration.

Existing high-lift device research extensively investigates aerodynamic performance with respect to flap configuration and positioning [8]. However, structural implications of design concepts remain insufficiently quantified. An efficient and mechanically consistent design workflow is therefore required to support early-phase decision-making. To close this gap, this article presents a workflow for rapid structural trade studies of TE devices. By combining the industry relevant CPACS-based geometry definitions, beam-element idealization, and automated sizing under aerodynamic and kinematic loads with prescribed deflection limits, the workflow enables consistent evaluation of multiple structural concepts, and efficient exploration of vast parametric design spaces. Structural sensitivities and mass trends can thus be quantified, supporting cross-disciplinary trade-offs and identification of favorable design regions, all during preliminary design. The link to the omega concept is demonstrated in the trade study presented in Section 3.1.2, where, for example, the influence of tilted spars on control-surface mass is quantified with respect to a conventional 2-spar solution.

The remainder of the paper is structured as follows. Section 2 describes the composition of the design workflow. Section 3 presents trade studies on evaluating support-station placement and internal reinforcement layout on representative inboard and outboard flaperons of a HAR wing. Section 4 summarizes the conclusions and outline future work.

2. Methodology: rapid structural concept evaluation

This workflow is developed for early-stage structural concept evaluation and trade studies of TE high-lift devices. It uses CPACS-based geometry definitions to parameterise design variables such as support-station placement and reinforcement layout details such as spar type, spacing, and relative rotation. The defined geometry is then idealized as beam elements using the PreDoCS solver [9]. This provides an appropriate level of fidelity for preliminary design, capturing the global stiffness and load paths required for structural sizing while retaining the efficiency needed for broad design-space exploration. Structural responses from the loaded beam model are subsequently used for sizing with lightworks, an internal DLR design framework [10]. Together, the beam-based analysis and automated sizing enable structural concepts to be evaluated on a mechanical basis rather than through purely geometric or empirical estimates. This streamlined workflow is illustrated in Fig. 3, with the detailed methodology for each component described in the following subsections.

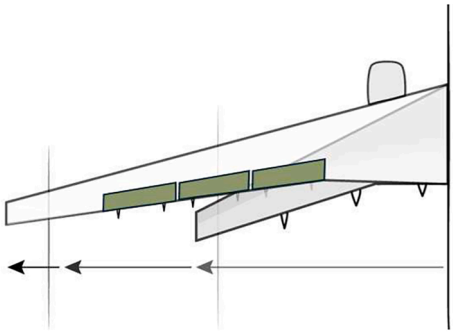


Fig. 1. High aspect ratio wing envisioned for future single-aisle aircraft.

2.1. Parametric flap geometry model using CPACS

The flap models used in this study are defined in CPACS (Common Parametric Aircraft Configuration Schema [11]), a standardized XML-based format for fully parametric aircraft description. CPACS enables a consistent representation of geometry, structural layout, materials, and loads. It is widely applied in multidisciplinary aircraft design and analysis [12].

Airfoil profiles are defined by a set of 2D contour coordinates and can be scaled in chord length and thickness. The desired airfoils are then assigned to defined spanwise sections and scaled according to the local chord length and relative thickness. As such, the aerodynamic outer surface of the flaperon is described as a smooth and fully parametric surface definition (Fig. 4).

Beyond the outer mold line, the CPACS model defines the internal structure, including spars and shell components. The stiffening concept is specified through the number of spars, their chordwise placement and orientation, while the shells can be defined as monolithic or stiffened. Each component is subdivided into design regions with assigned composite properties or homogenized sub-laminates for sizing (refer to Table A.1). Upon sizing, the resulting laminates are written back to the same file, enabling consistent data exchange.

External loads are prescribed in the CPACS file as distributed force and moment vectors for multiple load cases. It is defined along a spanwise reference axis. Boundary conditions are specified accordingly to ensure consistent and physically meaningful load application in the subsequent structural analysis.

This parametric modeling approach allows systematic geometric and structural variation while maintaining coherence between aerodynamic shape, structural layout, and load definition. The CPACS models used in this study are publicly available in a dedicated repository [22].

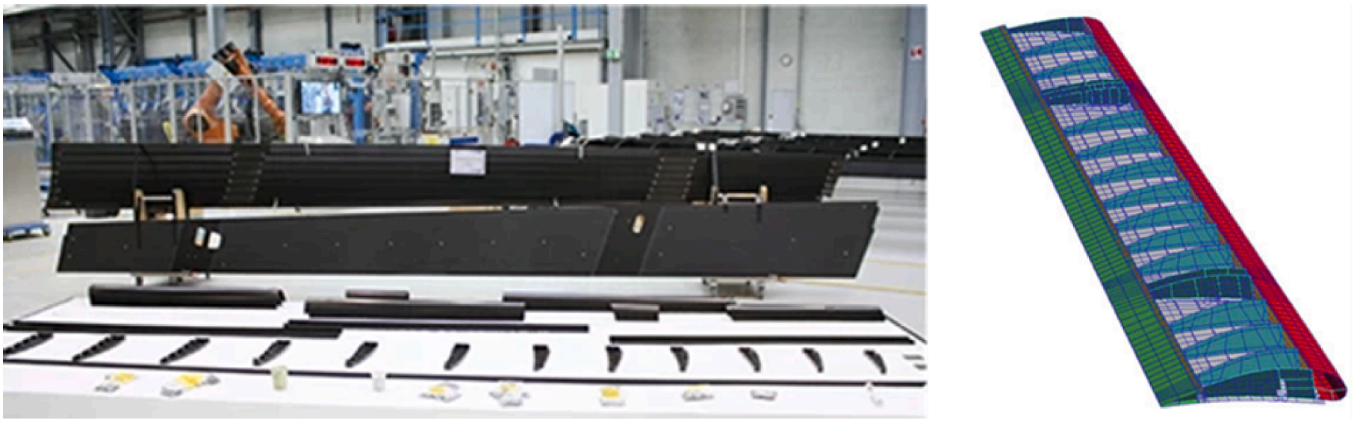
2.2. Design loads and boundary conditions

In preliminary design, the flap is analyzed independent of the wing, i.e., wing–flap interaction is not considered. For the structural assessment of high-lift devices, aerodynamic loads are expressed in the local device coordinate system. The resulting force components normal (N) and tangential (T), together with the torsional moment (M), form the NTM load set.

From Computational Fluid Dynamics, a resultant aerodynamic force vector is first obtained in the aircraft (AC) coordinate system, acting at the center of pressure (CoP) of the flap. This vector corresponds to critical load cases at a given airspeed and flap deflection angle. It is then transformed into the local device coordinate system and shifted to its origin [13]. The offset from the CoP to the device reference axis introduces an additional moment (cross product of the force vector and the offset vector). As such, the resulting NTM components are consistently expressed in the local device system (Fig. 5).

The resulting NTM components are distributed spanwise along the loads reference axis defined in CPACS, scaled with the local chord length to represent sectional loading. No loads are applied at the flap tips and the kinematic attachment points in order to account for local load reduction due to flow separation or the presence of track fairings (as shown in Fig. 6).

Support conditions at the flap tracks are idealized using nodal boundary conditions. All translational degrees of freedom are constrained, while rotation about the chordwise axis is left free to reflect the bending allowed by the spherical bearings connecting the kinematics to the flap.



(a) Today's differential concept for an A321 composite flap [4] and corresponding design concept [5]



(b) High-TRL modular composite flap concepts: Composite Multi-Spar Flap (CMF, 2015) ©Radius Engineering [6], Advanced Multi-Cell Flap (AMF, 2021) ©FACC [7], and DLR's omega-backbone concept for the F25 outboard flaperon-3 (from left to right)

Fig. 2. Overview of conventional and alternative composite flap architectures.

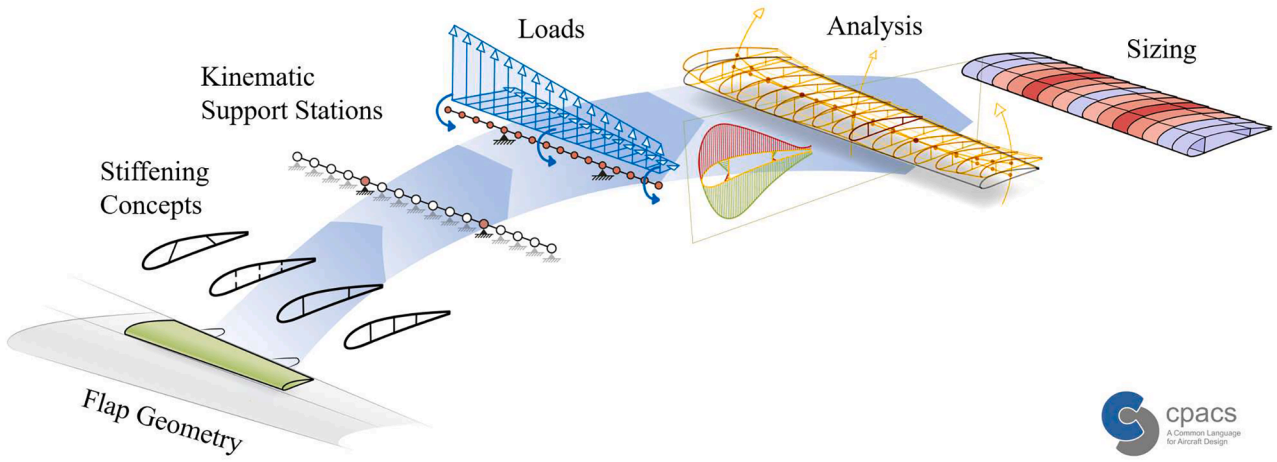


Fig. 3. Overview of the preliminary structural design workflow for high-lift devices.

In CPACS notation, this corresponds to a constraint vector $(0,0,0,1,0,0)$ in the coordinate system $(u_x, u_y, u_z, \theta_x, \theta_y, \theta_z)$, where 0 denotes a restrained and 1 a free degree of freedom.

In addition to the nominal aerodynamic load case, an off-nominal kinematic failure scenario is considered. As illustrated in Fig. 7 for a dropped-hinge kinematic, this is when actuation continues despite a failed actuator. To model this, one flap track is fully constrained as before, while the other support carries the full moment from the corresponding NTM load set. Complementary failure cases are generated by considering each attachment point in turn as failing while the others remain constrained.[1] This enables consistent evaluation of load redistribution and structural compliance in off-nominal scenarios.

2.3. Beam idealisation and analysis

To determine the mechanical response under loading, the flaperon is idealized as a one-dimensional beam and analyzed using the solver PreDoCS, previously validated against commercial FE solvers [9]. The beam-based idealization efficiently captures global stiffness and load paths through equivalent sectional properties.[2] It is therefore suited to

[1] Two complementary cases of kinematic failure, for a flap with two supports.

[2] The beam axis follows the CPACS y-direction (different from the native PreDoCS convention [9]) for consistency within this article.

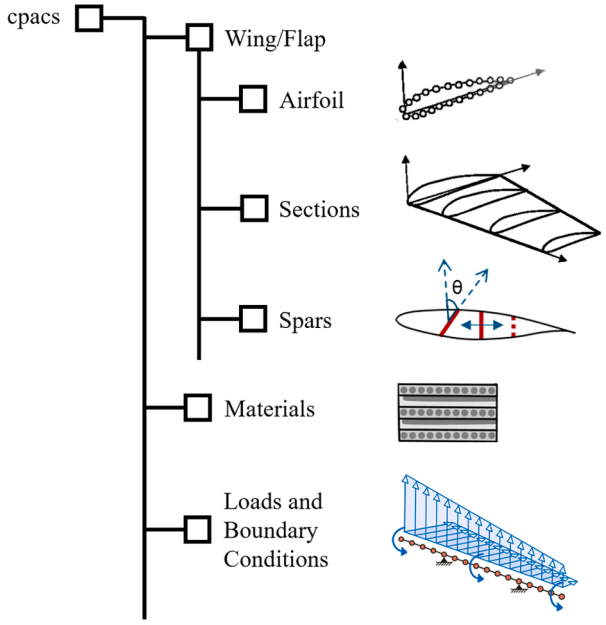


Fig. 4. Data structure and contents of a CPACS file.

rapid exploration of structural concepts in preliminary design, while detailed local behavior around supports or joints requires higher-fidelity analysis. The procedure includes: deriving cross-sectional properties, applying external loads, solving the beam finite element model, and recovering sectional and panel loads for sizing. Fig. 8 provides a concise illustration of this process.

As described in Section 2.1, the CPACS file provides the geometric description, material properties, and structural layout of the flaperon along the span. Based on this information, an analytical thin-walled cross-sectional analysis is performed at discrete spanwise locations to determine the sectional stiffness matrix:

$$\mathbf{K}_{\text{cs}} \in \mathbb{R}^{7\times 7}, \tag{1}$$

This matrix accounts for axial, bending, shear, torsional, warping stiffness, and coupling terms. Based on this sectional stiffness matrix, the beam constitutive law with generalized strains $\boldsymbol{\epsilon}_{\text{gen}}$ and the corresponding sectional internal force vector $\mathbf{F}$ reads as follows:

$$\mathbf{F} = \mathbf{K}_{\text{cs}}\,\boldsymbol{\epsilon}_{\text{gen}}, \qquad \boldsymbol{\epsilon}_{\text{gen}} = \begin{bmatrix} \epsilon_y \\ \kappa_x \\ \kappa_z \\ \kappa_y \\ \gamma_x \\ \gamma_z \\ \omega' \end{bmatrix}, \quad \mathbf{F} = \begin{bmatrix} N \\ M_x \\ M_z \\ T \\ V_x \\ V_z \\ M_\omega \end{bmatrix}. \tag{2}$$

Here, N is the axial force along the beam axis; M_x, M_z are the bending moments about x and y axes respectively; T the Saint-Venant torsional moment about y-axis; V_x, V_z the transverse shear forces; and M_ω the bimoment due to restrained warping. The corresponding generalized strains are the axial strain along beam-axis ϵ_y, bending curvatures κ_x, κ_z, the torsional curvature κ_y, transverse shear strains γ_x, γ_z, and the derivative of the warping displacement ω'.

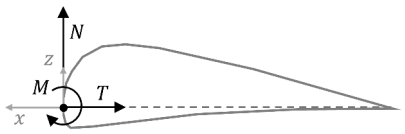


Fig. 5. NTM loads applied at the leading edge in the CPACS coordinate system (x downstream, y toward the right wing, z upward).

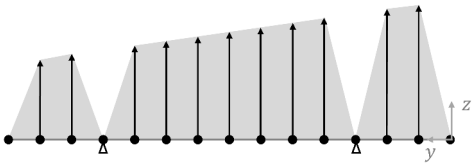


Fig. 6. Spanwise distribution of NTM loads as a function of local chord length.

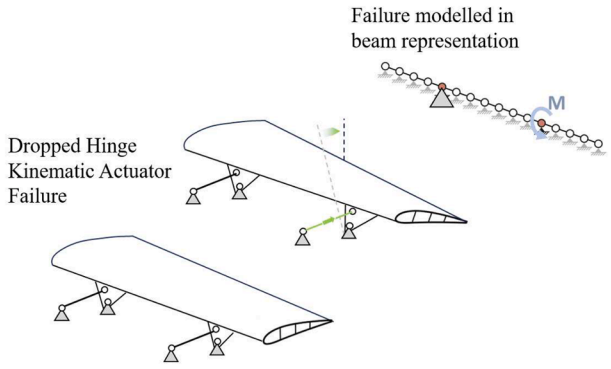


Fig. 7. Dropped-Hinge kinematic failure case and corresponding simplified structural model (see also [14]).

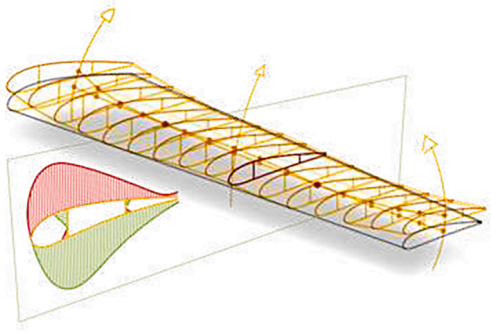


Fig. 8. Beam idealization of the flaperon and recovery of sectional and panel loads using PreDoCS.

$\mathbf{F}$ is obtained by solving the global beam equilibrium in a finite element formulation. Spanwise external loads (as defined in Section 2.2) from CPACS are applied as nodal forces and moments:

$$F_x(y),\ F_z(y),\ F_y(y),\ M_x(y),\ M_z(y),\ M_y(y), \tag{3}$$

These loads are defined along the load reference axis defined in CPACS. These spanwise load application points are considered the nodes of the 1D beam idealization. The sectional stiffness matrices evaluated at the nodes are assembled into a global Timoshenko beam system (see [15] for 1D FE-model derived from the cross-sectional formulation):

$$\mathbf{K}_{\text{glob}}\,\mathbf{u} = \mathbf{F}_{\text{glob}}. \tag{4}$$

with element-level form $K_e\,\mathbf{u}_e = \mathbf{F}_e$, where K_e contains the sectional stiffness contributions and beam shape functions. Solving this system yields the nodal displacement field $\mathbf{u}(y)$, from which generalized strains follow:

$$\boldsymbol{\epsilon}_{\text{gen}}(y) = \mathbf{B}(y)\,\mathbf{u}(y), \tag{5}$$

$\mathbf{B}(y)$ denotes the beam strain–displacement matrix. Now, Sectional forces $\mathbf{F}(y)$ can be calculated by substituting $\boldsymbol{\epsilon}_{\text{gen}}(y)$ in Eq. (2).[3]

[3] Axial forces and bending moments are referenced to the cross-sectional origin; shear forces and torsion to the shear center.

Using Jung's recovery relations [16], the generalized strain state at each node is transformed into local stresses within the cross section. Integration through the wall thickness yields the contour forces:

$$n_y(s,y) = \int_{-t/2}^{t/2} \sigma_y(s,n,y)\,\mathrm{d}n, \tag{6}$$

$$q(s,y) = \int_{-t/2}^{t/2} \tau_{ys}(s,n,y)\,\mathrm{d}n, \tag{7}$$

where s denotes the contour coordinate and n the wall-normal direction. This serves as the relevant membrane forces and shear flows for structural sizing of the panels and spars, as explained in the following subsection.

2.4. Structural sizing with fully stressed design criteria

Structural sizing is performed using the DLR in-house optimisation framework, lightworks [10]. A panel-based sub model is generated from the CPACS description and subdivided into desired number of design regions. Each region is modeled with Classical Lamination Theory, providing an equivalent composite stiffness representation. As illustrated in Fig. 9, the sectional loads from PreDoCS (in Section 2.3) are mapped onto these regions to evaluate strain and stability criteria to accordingly size the laminate. Here, r denotes the resultant membrane and shear flows (Eq. (6)).

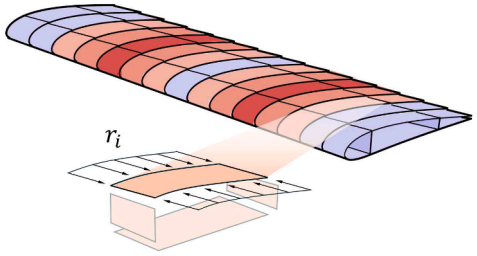


Fig. 9. Membrane and shear flows r_i recovered from PreDoCS and used to panel sizing in lightworks.

For quick sizing, lightworks is configured to follow a fully stressed design (FSD) approach [17,18], where laminate thickness is iteratively updated until all criteria are satisfied with minimal structural weight. In this study predefined Quad laminates are used as starting points, as summarized in Table A.1. For the i^{th} design region, the thickness update in iteration k is:

$$t_i^{(k+1)} = t_i^{(k)} \cdot s_i^{(k)}, \tag{8}$$

$$s_i^{(k)} = \max\left[\left(\frac{|r_i^{(k)}|}{r_{\mathrm{crit},i}}\right)^{1/3}, \frac{|\varepsilon_i^{(k)}|}{\varepsilon_{\mathrm{crit},i}}\right], \tag{9}$$

Here, r_i and ε_i are the local load and strain measures respectively, across all load cases. Critical buckling load $r_{\mathrm{crit},i}$, is computed as described in Appendix B, and critical strain $\varepsilon_{\mathrm{crit},i}$, is based on the maximum strain criterion. The buckling contribution in Eq. (9) enters the scaling factor with exponent $1/3$ to linearise its cubic influence on deflection, while the strain contribution acts linearly.

From iteration $k \geq 3$, a global deflection constraint w_{crit} is enforced. If the maximum deflection $w^{(k)}$ exceeds a given limit, all laminate thicknesses are uniformly scaled:

$$t_i^{(k+1)} = t_i^{(k)} \cdot s_i^{(k)} \cdot \Gamma^{(k)}, \tag{10}$$

$$\Gamma^{(k)} = \max\left(1, \frac{|w^{(k)}|}{w_{\mathrm{crit}}}\right), \tag{11}$$

This is done only after three iterations, to preserve local FSD behavior while eventually enforcing global deflection limits.

Table 1
DLR-F25 wing flaperons considered in this study [2] (wing v04, HL layout 015).

Parameter	Flaperon-1	Flaperon-3
Span	1.756 m	3.644 m
Min/Max Chord	0.979-1.088 m	0.335-0.518 m
Min/Max Section Height	0.190-0.206 m	0.07-0.12 m
NTM Loads	[72292 N, 66 N, 25,037 Nm]	[65641 N, 67 N, 9730 Nm]

Table 2
DOE for spanwise kinematic support-station locations.

Support Station	Spanwise Position (% of span)
Inboard	5, 10, 15, 20, 25, 30, 35, 40, 45
Outboard	55, 60, 65, 70, 75, 80, 85, 90, 95

The absolute structural mass depends on the assumed sublaminate properties, so alternative stacks or material systems may shift the quantitative optima. Nevertheless, given the scale and loading of the secondary structure (Section 2.2), the influence of laminate definition is assumed to be secondary to that of geometry in governing the load paths.

The complete workflow from reading CPACS geometry to a converged, compliant flap requires two to three minutes on a standard office laptop. This computational efficiency, while accounting for key structural criteria, enables rapid early-stage parametric studies to identify key critical design drivers.

3. Parameter studies on HAR-wing flaperons

Using the proposed workflow, trade studies were conducted on the DLR-F25 flaperons to identify optimal kinematic support station locations and stiffening concepts. A common design rule of thumb places both supports and spars at the quartiles (25%, 75%) of span and chord, respectively. With this lightworks-based workflow, we now aim to show the sensitivity of structural mass is assessed w.r.t spanwise positioning of the supports and the chordwise positioning of the spars.

To highlight the geometry-induced differences, the study is carried out for two geometrically distinct flaperons of the DLR-F25 configuration: a slender outboard device (Flaperon-3) and a bulkier inboard device (Flaperon-1). Their CPACS models are provided in an open-source repository published together with this work [22]. Key geometric parameters are summarized in Table 1.

Both flaperons are subjected to identical sizing parameters in lightworks, including a global safety factor of 1.5 for buckling and strain criteria and a maximum allowable tip deflection of 10 mm. As explored in a previous study [19], the loads are applied across 31 nodes, and each structural component is subdivided into 20 spanwise design regions, allowing discrete thickness variation.

The analysis proceeds in two steps. First, the slender outboard flaperon (Flaperon-3)(in Section 3.1) is examined to determine optimal support-station locations and reinforcement concepts. The same methodology is subsequently applied to the bulkier inboard flaperon (Flaperon-1)(in Section 3.2), enabling a direct comparison of geometry-driven sensitivities.

3.1. Slender outboard flaperon

The slender flaperon-3 serves as the reference case for the parameter study. Owing to its large aspect ratio, it is expected to exhibit high sensitivity to unsupported lengths and reinforcement layout. The study is structured in two stages: first, the optimal spanwise support-station locations are determined; second, internal reinforcement concepts are varied while keeping the support positions fixed.

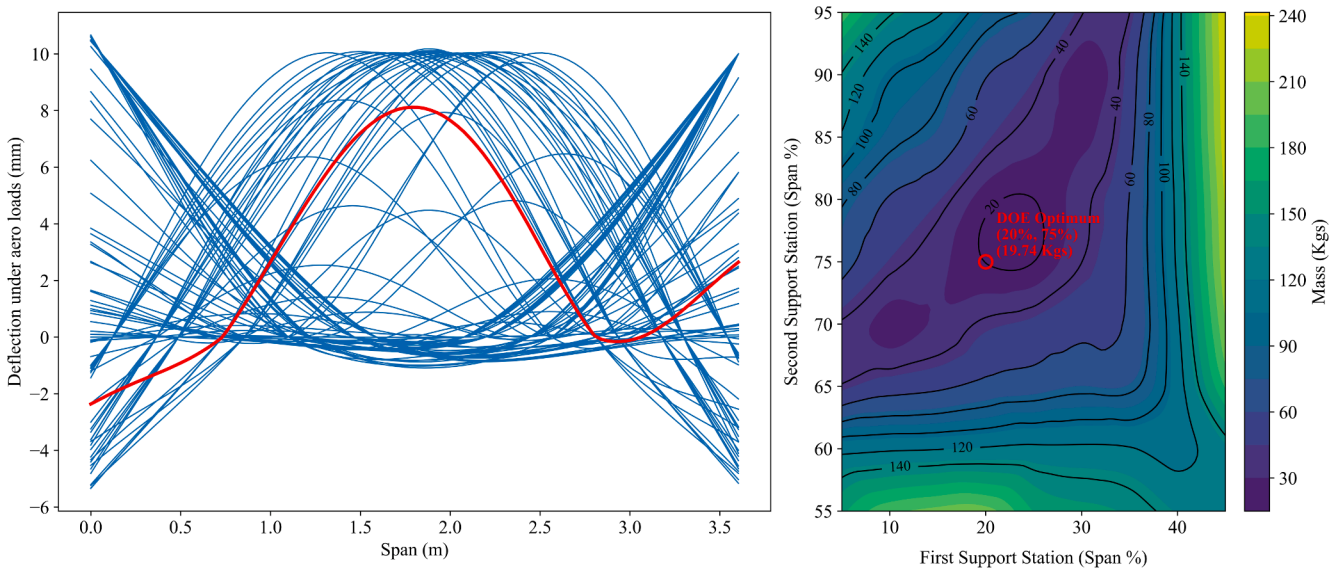


Fig. 10. Mass and deflection trends of Flaperon-3 for varying support station locations.

Table 3
DOE for spar reinforcement layouts.

Concept	No. of Spars	Rotation (∘)	Candidate Positions (% chord)	Total Combinations
2-Spar	2	0		$\binom{9}{2} = 36$
Omega	2	10, 20, 30	10, 20, 30, 40, 50, 60, 70, 80, 90	$3 * \binom{9}{2} = 108$
3-Spar	3	0		$\binom{9}{3} = 84$

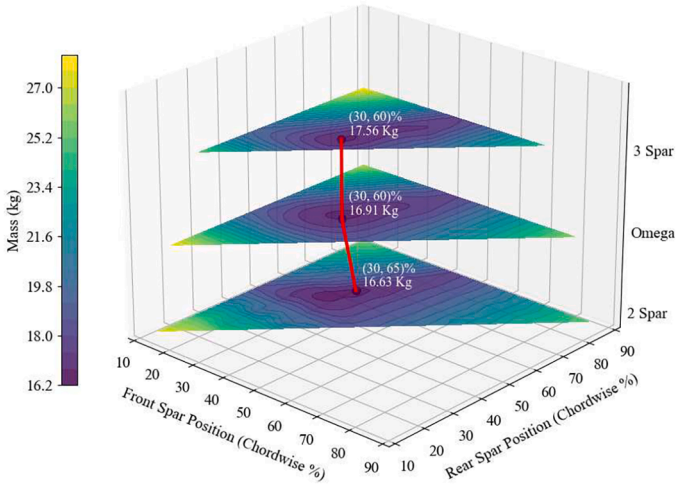


Fig. 11. Mass sensitivity of Flaperon-3 to reinforcement layouts, with lightest configuration of each concept traced in red. (For interpretation of the references to color in this figure legend, the reader is referred to the web version of this article.)

Table 4
Optimal structural configurations and mass savings relative to the reference quartile configuration (supports at 25/75% span and spars at 25/75% chord).

Flaperon	Parameter	Optimum	Mass (ref./opt.)	Saving
Flaperon-3	Supports (% span)	(20, 75)	19.74 / 16.63 kg	15%
	Spars (% chord)	(30, 65)		
Flaperon-1	Supports (% span)	(20, 75)	21.69 / 21.58 kg	23%
	Spars (% chord)	(30, 60)		

3.1.1. *Influence of support-station location*

From classical mechanics of a beam, bending deflection scales with the cube of the unsupported length. While internal reinforcement and section height also influence stiffness, the airfoil geometry largely fixes the section height, and reinforcement primarily affects local stiffness. In contrast, support placement directly controls unsupported lengths and therefore dominates global deflection behavior. Hence, to isolate the effect of reinforcements and independently analyze optimum support placement, a baseline two-spar configuration with spars fixed at 25% and 75% chord is adopted. This reduces problem dimensionality while preserving representative structural trends.

Support positions are treated as discrete variables corresponding to beam-node locations. Candidate spanwise positions are listed in Table 2. The 9 inboard support is restricted to the inner half of the span and the 9 outboard support to the outer half, ensuring physically meaningful configurations. All 81 combinations (e.g., 5–95, 10–90, etc.) form the design of experiments (DOE).

By sizing the flaperon for all these combinations, the design space was systematically explored. This took around 4 h of computational effort and the results are summarized in Fig. 10, with the corresponding deflection curves for all flaperons, and a mass contour plot with the inboard and outboard support locations as the axes.

Across most configurations, the deflection profiles exhibited a characteristic “U”-shape along the span. However, whether the “U” opened upward or downward depended directly on the relative placement of the support stations. Configurations with supports placed very close together or very far apart, have their maximum deflections capped near the 10mm limit. Since upward deflection is driven solely by the NTM loads, these configurations are aerodynamic-driven, and the FSD procedure compensates by increasing laminate thickness to satisfy the deflection constraint. The remaining design combinations are driven by the kinematic failure load case.

The mass contour plot indicates optimal support locations at approximately 20–25% span (inboard) and 75–80% span (outboard). Within

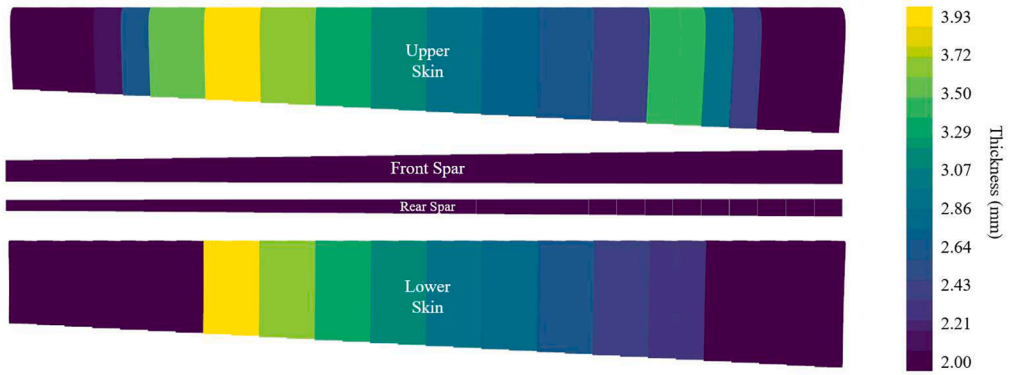


Fig. 12. Minimum-mass configuration of Flaperon-3: supports at (20%, 75%) span, and two spars at (30%, 65%) chord.

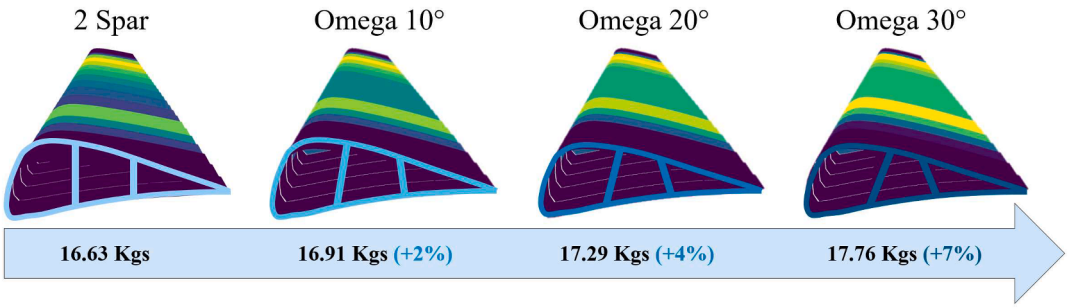


Fig. 13. Quantifying mass penalty of Flaperon-3 by rotating spars for ease of production (Omega configuration).

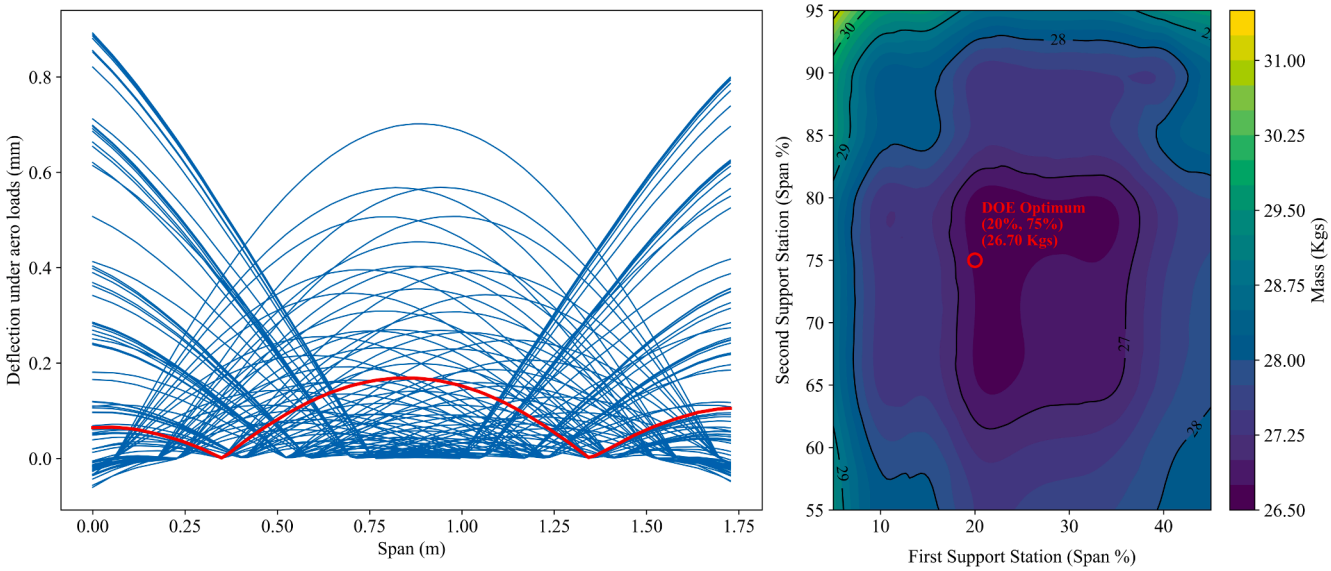


Fig. 14. Mass and deflection trends of Flaperon-1 for varying support station locations.

the discrete DOE, the combination (20%, 75%) yields the lowest mass of 19.74 kg. This is close to the conventional quartile assumption (25%, 75%) at 19.93 kg, but alternative configurations of comparable mass exist. Notably, when the distance between supports is approximately 60% of the span, the structural mass remains near 20 kg, demonstrating a range of desirable solutions apart from the conventional (25%, 75%).

3.1.2. *Influence of reinforcement layout*

With support stations fixed at (20%, 75%), the influence of internal reinforcement is investigated. The study quantifies the effect of spar number, chordwise spacing, and rotation under identical boundary conditions. The corresponding design of experiments (DOE) is summarized in Table 3.

Nine discrete chordwise locations (10–90%) are defined. Two- and three-spar layouts are generated by combinatorial selection, yielding $\binom{9}{2}$ and $\binom{9}{3}$ configurations, respectively.[4] For the omega concept, the same combinations are considered with rotation angles of 10°, 20°, and 30°, excluding geometrically infeasible cases (spar intersection). Chordwise position and rotation are defined at the spar midpoint; the front spar

[4] $\binom{n}{k} = n!/(k!(n-k)!)$ denotes the number of unordered selections of k items from n.

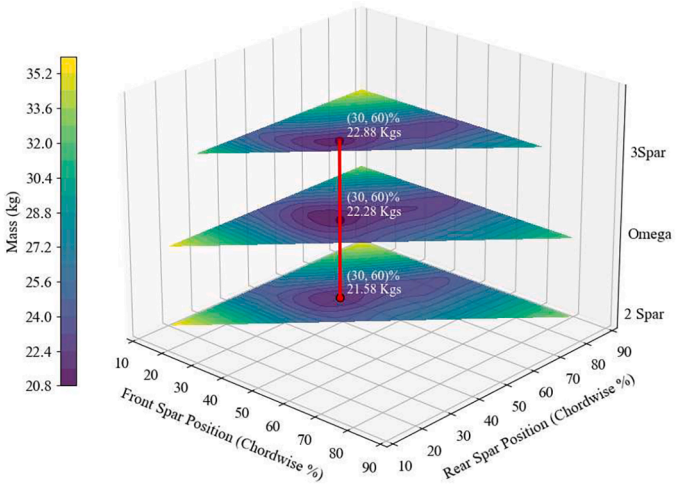


Fig. 15. Mass sensitivity of Flaperon-1 to reinforcement layouts, with lightest configuration of each concept traced in red. (For interpretation of the references to color in this figure legend, the reader is referred to the web version of this article.)

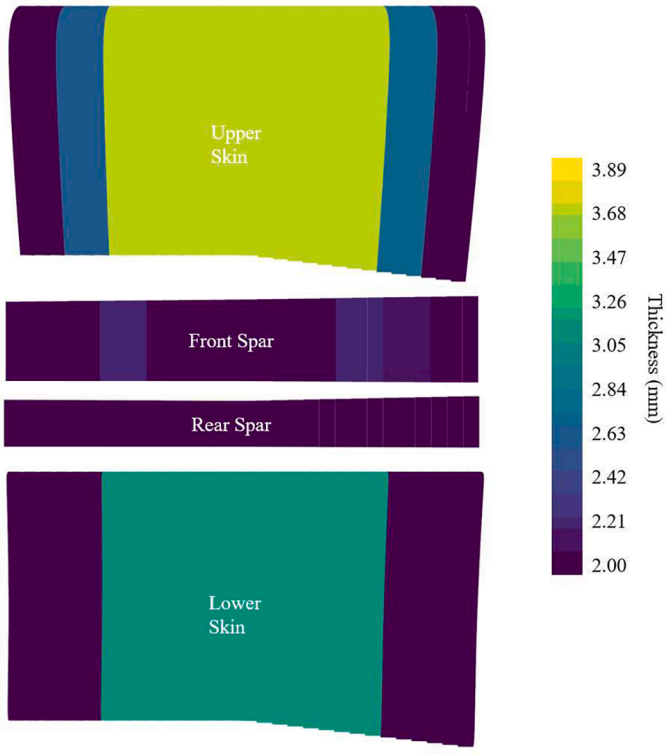


Fig. 16. Minimum-mass configuration of Flaperon-1: Supports at (20%, 75%) span, and two spars at (30%, 60%) chord.

is rotated clockwise, the rear spar counterclockwise. All 228 configurations are sized in around 8 h, and the resulting masses are shown in Fig. 11.

The stacked contour plots, map front and rear spar positions to structural mass for each concept. To represent the three-spar concept in two dimensions, only the minimum-mass configuration for each front–rear pair is plotted. Independent of reinforcement concept, the optimum front and rear spar positions consistently occur near 30% and 60% chord. he smooth, convex contours indicate clear sensitivity to spar placement and stable structural trends.

As shown in Fig. 12, the two-spar concept at (30%, 65%) achieves the minimum mass of 16.63 kg, with laminate thickness concentrated around the kinematic supports. The kinematic failure case heavily loads both skins; however, due to upward bending under aerodynamic loading, the lower skin is less buckling-critical and therefore marginally thinner. This result represents a 15% reduction compared to the conventional (25%, 75%) layout at 19.74kg.

Introducing a third spar enhances skin buckling resistance and can reduce the required laminate thickness. The best three-spar design is found to be (30%, 50%, 60%). However, the added spar itself, even at minimum allowable thickness, leads to a higher overall mass compared to the two-spar layout. The omega configuration is likewise two to seven % heavier than the optimal two-spar layout, due to spar rotation. While structurally less efficient, the rotated spars simplify manufacturing and improve accessibility within the slender structure. This trade-off is quantified in Fig. 13. As such, this workflow enables informed evaluation of structural efficiency versus production benefits at ease.

3.2. Bulky inboard flaperon

The parameter studies are repeated for Flaperon-1 to assess geometry-driven effects. By following the same DOE as before, all results can be generated in around 12 h. The resulting mass and axial deflection trends for varying support locations in Flaperon-1 are shown in Fig. 14.

Compared to Flaperon-3, the bulky Flaperon-1 exhibits reduced sensitivity to support placement. Moreover, the deflection constraint remains inactive for every design combination, meaning the design is solely driven by the kinematic failure load case. This is attributed to its shorter span and larger section height. Therefore, for flaperon-1, a broader range of support locations yields comparable mass: approximately 20–40% inboard and 60–80% outboard of span.

The reinforcement parameter study is repeated using the same DOE (as Table 3) and support locations fixed at (20%, 75%) span. As seen in Fig. 15, the optimal spar once again positions cluster near (30%, 60%) chord. Moreover, the loads are once again resolved around the kinematic supports, leading to locally increased laminate thickness, as seen in Fig. 16. These results indicate that, once support positions are fixed, the internal reinforcement behavior is largely geometry-independent.

With Fig. 17, a direct comparison of both flaperons are shown. The slender flaperon-3 favors widely spaced supports(õ60% of span length) and exhibits a sharply defined low-mass region. In contrast, the bulky flaperon-1 is less sensitive to support placement and allows a wider range of structurally competitive solutions (20-40%, 60–80% of span).

Among the investigated design parameters, support-station placement had the strongest influence on structural mass, particularly for the slender outboard flaperon. The mass savings achieved by optimizing the support and spar positions relative to conventional quartile placement are presented in Table 4. The present study treats the flaperon independently of the wing, consistent with its preliminary-design objective. The wing–flap interaction may shift the absolute load levels and resulting mass, but the identified geometric sensitivities are expected to remain.

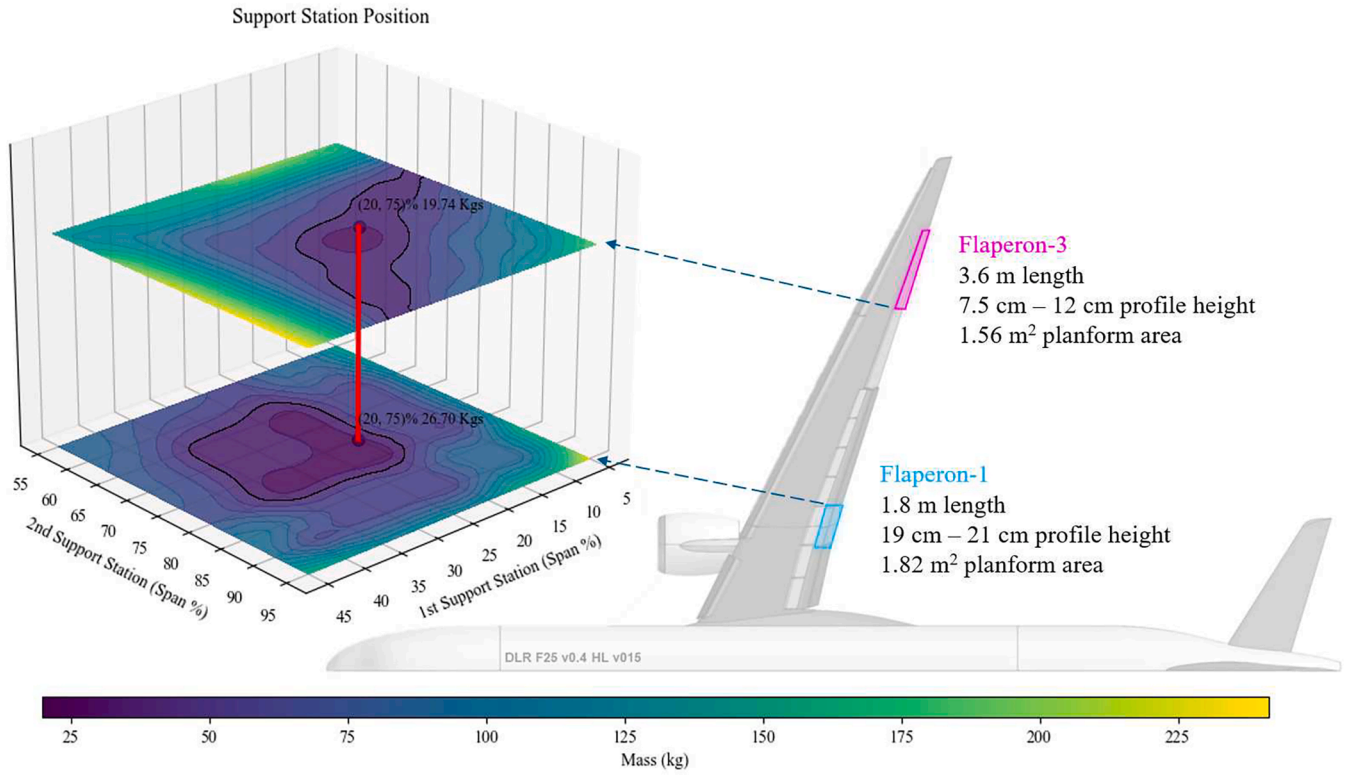


Fig. 17. Difference in optimum configurations of Flaperons 1 and 3 of the DLR-F25.

4. Conclusion

This article presents a lightworks-based workflow for systematic structural trade studies of control surfaces. Combining the modular optimisation framework lightworks [10] with the efficient beam solver PreDoCS [9], the approach enables rapid, mechanically consistent exploration of design spaces for high-lift devices. CPACS-based input parameterisation allows flexible definition of arbitrary geometries, and load cases for sizing: aerodynamic (NTM) loads, and kinematic failure scenarios. Strength, stability, and explicit deflection limits can be set for target aerodynamic gap quality.

Extending prior material selection and thickness variation studies [19], the workflow now explores support-station placement and internal reinforcement layout across flaperons of varying geometries. This was done by comparing the sized inboard and outboard flaperons of the High Aspect Ratio DLR-F25 wing. The results demonstrate that optimal configurations are geometry-specific. Upon sizing with homogenized laminates, slender profiles (flaperon-3) exhibit narrow low-mass design regions and strong sensitivity to support spacing, whereas shorter, bulkier profiles (flaperon-1) allow broader range of competitive solutions and are completely driven by the kinematic failure load case. While based on the DLR-F25 flaperons, the observed trends can be generalized as follows. The longer span and smaller section height of slender profiles increase their sensitivity to unsupported length and make deflection more critical, whereas shorter, deeper profiles are less sensitive to unsupported length, preventing the deflection constraint from becoming active.

An individual design concept can be sized in $\tilde{3}$ min, enabling rigorous parametric studies ($\tilde{1}$2 h) to identify favorable design regions and guide architectural decisions beyond conventional quartile placements (25%,75%). Such studies promote better cross-discipline exchanges during preliminary design, and help make context-specific and informed decisions.

Furthermore, production-driven concepts such as rotated (omega) spars can be quantitatively compared to structurally optimal two-spar layouts. The associated mass penalties are evaluated, enabling justified trade-offs between structural efficiency and manufacturability.

5. Outlook

Overall, the workflow provides a quick setup for early-stage architecture studies. It enables consistent variation of geometry, boundary conditions, load assumptions, material models, and optimisation strategies. In future studies, it can be readily extended to assess configurations with additional support stations, alternative stiffening concepts, and refined criteria beyond the current panel-based buckling treatment of leading & trailing edges.

Rapid concept evaluation is achieved using Fully Stressed Design (FSD). While efficient and suitable to identify global trends, it may be suboptimal for structures with pronounced parallel load paths [18]. The underlying lightworks framework supports gradient-based thickness optimisation and even directional stiffness tailoring via lamination parameters [10]. Thus, FSD-based concept screening can be seamlessly complemented by higher-fidelity optimisation and extended toward coupled wing–flap structural interaction.

CRediT authorship contribution statement

Rakshith Manikandan: Writing – review & editing, Writing – original draft, Validation, Software, Methodology, Investigation, Conceptualization; **David Zerbst:** Writing – review & editing, Writing – original draft, Validation, Methodology; **Erik Kappel:** Writing – review & editing, Validation, Formal analysis, Conceptualization; **Lennart Tönjes:** Validation, Software, Methodology; **Edgar Werthen:** Methodology; **Sascha Dähne:** Software, Formal analysis; **Christian Hühne:** Supervision, Funding acquisition, Conceptualization.

Declaration of competing interest

The authors declare that they have no known competing financial interests or personal relationships that could have appeared to influence the work reported in this paper.

Acknowledgments

The authors would like to thank Daniel Hardt for insightful discussions on beam modeling, alongside Niko Bier and Sven Pülm for their clarifications on aerodynamic load distribution across flaps. This work is supported by the EU-funded project 101101974-UP Wing (Ultra Performance Wing) and is supported by the Clean Aviation Joint Undertaking and its members. We would also like to acknowledge the funding by the Deutsche Forschungsgemeinschaft (DFG, German Research Foundation) under Germany´s Collaborative Research Center – CRC 1463/2 - Integrated design and operation methodology for offshore megastructures – Project-ID 434502799.

Data availability

The CPACS data required to describe the flaperons in this study are available to download from [22]. I have shared a link to the required data.

Appendix A. Material properties

The material properties of the prepreg used in this study are tabulated as follows in:

Table A.1
Material properties of M21E-IMA [20], allowables and applied composite layups.

Material Properties	
E_1 [Pa]	1.54×10^{11}
E_2 [Pa]	8.50×10^{9}
G_{12} [Pa]	4.20×10^{9}
ν	0.35
ρ [kg/m^3]	1580
Strain Allowables	
$\varepsilon_{1c}, \varepsilon_{1t}, \varepsilon_{2c}, \varepsilon_{2t}$ [-]	0.004
γ_{12} [-]	0.007
Predefined Composite Layup Blocks	
Shells	$[45°, 90°, -45°, 0°, 0°]_S$
Spars	$[45°, -45°, -45°, 45°, 0°]_S$

For a quick sizing of a flaperons, the fully stressed design (FSD) approach was used in this study. Predefined sublaminates are defined for the shells and skins appropriately. The thicknesses of these sublaminates are iteratively varied by the FSD process. For the skins, a 0° rich laminate ($[45°, 90°, -45°, 0°, 0°]_S$) provides near quasi-isotropic behavior, albeit with enhanced axial stiffness. Spars, experiences more shear-dominated loads. Therefore, they are assigned a 45° dominant laminate ($[45°, -45°, -45°, 45°, 0°]_S$) which retains some axial stiffness via 0° plies. Any alternative sublaminate can also be conveniently defined using the *CPACS* input, for example, a sublaminate with a minimum of 10% ply count for 0°, ±45° and 90° plies in the laminate.

Appendix B. Buckling analysis

The buckling behavior of a given laminated composite panel is calculated using analytical formulations from the HSB Handbook [21]. As detailed in the following subsections, the critical loads for compressive and shear buckling are computed separately, and then combined using an interaction criterion.

Compression buckling (HSB 45111-08)

The following relation is used to compute the critical buckling load per unit width under uniaxial compression:

$$r_{x,\mathrm{cr}} = k_x(\bar{\alpha}, \beta)\left(\frac{\pi}{b}\right)^2 \sqrt{D_{11} D_{22}} \tag{B.1}$$

$$\bar{\alpha} = \frac{a}{b}\sqrt[4]{\frac{D_{22}}{D_{11}}}$$

$$\beta = \frac{D_{12} + 2D_{66}}{\sqrt{D_{11} D_{22}}}$$

In this relation, x refers to the axis along which the highest principal load is observed.

Shear buckling (HSB 45112-02)

The following relation is used to calculate the critical buckling load per unit width under pure in-plane shear:

$$r_{s,\mathrm{cr}} = k_s(\beta)\left(\frac{\pi}{b}\right)^2 \sqrt[4]{D_{11} D_{22}^3} \tag{B.2}$$

In this relation, a and b represent a panel length and width, respectively, and $D_{i,j}$ are components of the flexural stiffness matrix. k_x and k_s are the buckling coefficients, obtained from standard reference plots of HSB [21]. For combined loading (compression and shear), the above-calculated critical loads are appropriately combined using the following relation:

$$R_x + R_s^2 \leq 1 \tag{B.3}$$

R can be defined as the ratio between applied and critical loads.

References

[1] M. Abu-Zurayk, A. DeBlois, J. Brezillon, B.D. Phillips, R. Petersson, R. llamas, C. Ilic, E. Aretskin-Hariton, J.W. Chapman, P. Wegener, J. Himisch, M. Schulze, J. Häßy, S. Dähne, C. Conlan-Smith, J. Singh, S. Wöhler, C. Blondeau, M. Meheut, S. Geisbauer, S. Görtz, Establishing a joint research-industry MDO benchmark based on the DLR-F25 aircraft configuration, in: AIAA SCITECH 2026 Forum, AIAA SciTech Forum, American Institute of Aeronautics and Astronautics, Orlando, Florida, USA, 2026. https://arc.aiaa.org/doi/10.2514/6.2026-0763.

[2] DLR, DLR research baseline F25, 2025. https://www.digital-hangar.de/portfolio/dlr-f25/.

[3] Airbus, Airbus reports full-year (FY) 2025 results, 2025, (Accessed: Date). Press release, https://www.airbus.com/en/newsroom/press-releases/2026-02-airbus-reports-full-year-fy-2025-results.

[4] G. Gardiner, Reducing manufacturing cost via RTM, CompositesWorld (2015). https://www.compositesworld.com/articles/reducing-manufacturing-cost-via-rtm.

[5] U.P. Breuer, Flap Design Case Study. In: Commercial Aircraft Composite Technology, Springer, 2016.

[6] R. Engineering, Airbus A320 outboard multi-spar flap, (2025). https://www.radiuseng.com/net_shape_composites{#}.

[7] F.-M. Sendner, G. Schneiderbauer, "Wing of tomorrow": FACC und airbus entwickeln Flügel der Zukunft, (2021). https://www.facc.com/de/news/wing-of-tomorrow-facc-und-airbus-entwickeln-fluegel-der-zukunft/.

[8] P. Radha Krishnan, R. Mukesh, I. Hasan, P. Booma Devi, W.A. Alebachew, Comparative study and aerodynamic analysis of rectangular wing using high-lift systems, Int. J. Aerosp. Eng. 2023 (2023) 5813557. https://doi.org/10.1155/2023/5813557

[9] E. Werthen, D. Hardt, C. Balzani, C. Hühne, Comparison of different cross-sectional approaches for the structural design and optimization of composite wind turbine blades based on beam models, Wind Energy Sci. 9 (7) (2024) 1465–1481. https://doi.org/10.5194/wes-9-1465-2024

[10] S. Dähne, E. Werthen, D. Zerbst, L. Tönjes, H. Traub, C. Hühne, Lightworks, a scientific research framework for the design of stiffened composite-panel structures using gradient-based optimization, Struct. Multidiscip. Optim. 67 (5) (2024) 70. https://doi.org/10.1007/s00158-024-03783-1

[11] M. Alder, E. Moerland, J. Jepsen, B. Nagel, Recent Advances in Establishing a Common Language for Aircraft Design with CPACS, Technical Report, DLR, 2020. https://elib.dlr.de/134341/

[12] M. Alder, E. Moerland, J. Jepsen, B. Nagel, Recent advances in establishing a common language for aircraft design with CPACS, in: Aerospace Europe Conference 2020, 2020. https://elib.dlr.de/134341/.

[13] S. Pülm, V. Handojo, R.B. Seidler, XRF1 high-lift load analysis of wing and high-lift system, in: 33rd Congress of the International Council of the Aeronautical Sciences (ICAS 2022), International Council of the Aeronautical Sciences, Stockholm, Sweden, 2022, pp. 1–18. Available at: DLR eLibrary, elib.dlr.de/191303/, https://www.icas.org/ICAS_ARCHIVE/ICAS2022/data/papers/ICAS2022_0228_paper.pdf.

[14] M. Lerch, F. Thielecke, Concepts for a safety device in conventional track-linkage kinematics to prevent skew in a single flap system, Deutscher Luft- und Raumfahrtkongress (DLRK) (DocumentID: 450068) (2017).
[15] K.-J. Bathe, Finite Element Procedures, Klaus-Jürgen Bathe, Watertown, MA, 2nd ed., 2014.
[16] S. Jung, V.T. Nagaraj, Structural behavior of thin- and thick-walled composite blades with multi-cell sections, in: 43rd AIAA/ASME/ASCE/AHS/ASC Structures, Structural Dynamics, and Materials Conference, American Institute of Aeronautics and Astronautics, Reston, Virigina, 2002.
[17] R. Razani, Behavior of fully stressed design of structures and its relationshipto minimum-weight design, AIAA J. 3 (12) (1965) 2262–2268.
[18] S.N. Patnaik, D.A. Hopkins, Optimality of a fully stressed design, Comput. Methods Appl. Mech. Eng. 165 (1–4) (1998) 215–221.
[19] R. Manikandan, D. Zerbst, E. Kappel, L. Tönjes, C. Hühne, Towards 'OptiFlap': preliminary structural sizing methodology for trailing-edge high-lift systems, Deutsche Gesellschaft für Luft- und Raumfahrt - Lilienthal-Oberth e.V., 2025.
[20] R. Talreja, J. Varna, Modeling Damage, Fatigue and Failure of Composite Materials, Elsevier, 2023.
[21] Working Group Structural Analysis (IASB), Aeronautical Engineering Handbook (LTH): Handbook for Structural Analysis (HSB).
[22] R. Manikandan, L. Tönjes, Rapid evaluation of structural concepts in preliminary design of trailing-edge high-lift devices: CPACS flaperon datasets and modified TiGL to consider rotated spars, 2026. https://doi.org/10.5281/zenodo.18923121.